Methods

Media and strains

All strains were grown at 30 °C in complete 2.0% (w/v) glucose (YPD) medium except where stated otherwise. Glucose restriction medium contained 0.5% or 0.1% glucose. Mild stress conditions were one of the following: defined medium (SD); amino acid restriction (SD lacking non-essential amino acids); salt stress (NaCl, 300 mM); heat stress (37 °C); sorbitol (1 M). In all experiments, auxotrophic markers were matched between strains by integrating empty vector. The copy number of integrated genes was determined by Southern blotting. Deletions were generated with a kan-MX6 PCR-based technique[16] and confirmed by PCR. Additional copies of *PNC1* were integrated as described previously[16]. The entire open reading frame and 700 bases of the upstream sequence of YLR285W were amplified from genomic DNA and cloned into pSP400, then sequenced and integrated as described previously[16]. A GFP cassette was integrated in frame at the 3′ end of the native *PNC1* gene as described previously[16]. The RFP–PTS1 (for peroxisomal targeting signal 1) plasmid (pSG421) was a gift from S. J. Gould (Johns Hopkins University). The coding region of human *NNMT* was subcloned from p91023(B), a gift from R. Weinshilboum (Mayo Clinic), into pSP400 downstream of the *ADH1* promoter. Strains derived from PSY316AT[16] were used for lifespan analysis. Strains derived from W303AR[11] were used for western blots, microscopy and silencing assays. W303AR *cdc25-10* was a gift from L. Guarente (MIT).

Yeast assays

Lifespan measurements were performed as described previously[16] except for the heat-stress experiments, in which strains were incubated after each dissection at 37 °C. Silencing was assayed as described previously[16].

Protein expression analysis

Strains were pretreated under the indicated conditions and grown to mid-exponential phase. Western blots were performed as described[16] with whole-cell extracts (75 μg). Proteins were detected with anti-GFP antibodies (Santa Cruz) or anti-actin antibodies (Chemicon). Fluorescent microscopy images were captured at the same exposure (1 s) at ×100 magnification with a Hamamatsu Orca100 CCD camera and processed with Openlab software. Cultures were grown in complete medium containing 0.5% glucose to enhance the detection of fluorescence.

Nicotinamidase activity assay

The activity of Pnc1 in extracts obtained from pretreated mid-exponential-phase cultures was determined as described previously[30]. In brief, 0.16 mg of protein was incubated with either 0 or 8 mM nicotinamide for 45 min at 30 °C in a final volume of 400 μl of 10 mM Tris-HCl pH 7.5, 150 mM NaCl and 1 mM $MgCl_2$. Pnc1 activity was determined by measuring the final concentration of the reaction product, ammonia, with an ammonia diagnostic kit (Sigma). Baseline ammonia was accounted for by subtracting a no-nicotinamide control. Nicotinamidase activity was expressed as nmol ammonia min^{-1} per mg total protein. Pnc1 activity was obtained by subtracting the background value for the *pnc1Δ* strain (0.06 ± 0.004 nmol min^{-1} per mg).

Received 11 February; accepted 20 March 2003; doi:10.1038/nature01578.

1. Lin, S. J., Defossez, P. A. & Guarente, L. Requirement of NAD and *SIR2* for life-span extension by calorie restriction in *Saccharomyces cerevisiae*. *Science* **289,** 2126–2128 (2000).
2. Bitterman, K. J., Anderson, R. M., Cohen, H. Y., Latorre-Esteves, M. & Sinclair, D. A. Inhibition of silencing and accelerated aging by nicotinamide, a putative negative regulator of yeast Sir2 and human SIRT1. *J. Biol. Chem.* **277,** 45099–45107 (2002).
3. Kaeberlein, M., Andalis, A. A., Fink, G. R. & Guarente, L. High osmolarity extends life span in *Saccharomyces cerevisiae* by a mechanism related to calorie restriction. *Mol. Cell. Biol.* **22,** 8056–8066 (2002).
4. Jiang, J. C., Jaruga, E., Repnevskaya, M. V. & Jazwinski, S. M. An intervention resembling caloric restriction prolongs life span and retards aging in yeast. *FASEB J.* **14,** 2135–2137 (2000).
5. Swiecilo, A., Krawiec, Z., Wawryn, J., Bartosz, G. & Bilinski, T. Effect of stress on the life span of the yeast *Saccharomyces cerevisiae*. *Acta Biochim. Pol.* **47,** 355–364 (2000).
6. Smith, J. S. *et al.* A phylogenetically conserved NAD^+-dependent protein deacetylase activity in the Sir2 protein family. *Proc. Natl Acad. Sci. USA* **97,** 6658–6663 (2000).
7. Imai, S., Armstrong, C. M., Kaeberlein, M. & Guarente, L. Transcriptional silencing and longevity protein Sir2 is an NAD-dependent histone deacetylase. *Nature* **403,** 795–800 (2000).
8. Tanny, J. C. & Moazed, D. Coupling of histone deacetylation to NAD breakdown by the yeast silencing protein Sir2: Evidence for acetyl transfer from substrate to an NAD breakdown product. *Proc. Natl Acad. Sci. USA* **98,** 415–420 (2001).
9. Landry, J. *et al.* The silencing protein Sir2 and its homologs are NAD-dependent protein deacetylases. *Proc. Natl Acad. Sci. USA* **97,** 5807–5811 (2000).
10. Kaeberlein, M., McVey, M. & Guarente, L. The Sir2/3/4 complex and Sir2 alone promote longevity in *Saccharomyces cerevisiae* by two different mechanisms. *Genes Dev.* **13,** 2570–2580 (1999).
11. Sinclair, D. A. & Guarente, L. Extrachromosomal rDNA circles—a cause of aging in yeast. *Cell* **91,** 1033–1042 (1997).
12. Tissenbaum, H. A. & Guarente, L. Increased dosage of a *sir-2* gene extends lifespan in *Caenorhabditis elegans*. *Nature* **410,** 227–230 (2001).
13. Rogina, B., Helfand, S. L. & Frankel, S. Longevity regulation by *Drosophila* Rpd3 deacetylase and caloric restriction. *Science* **298,** 1745 (2002).
14. Vaziri, H. *et al.* hSIR2(SIRT1) Functions as an NAD-dependent p53 deacetylase. *Cell* **107,** 149–159 (2001).
15. Luo, J. *et al.* Negative control of p53 by Sir2α promotes cell survival under stress. *Cell* **107,** 137–148 (2001).
16. Anderson, R. M. *et al.* Manipulation of a nuclear NAD^+ salvage pathway delays aging without altering steady-state NAD^+ levels. *J. Biol. Chem.* **277,** 18881–18890 (2002).
17. Landry, J., Slama, J. T. & Sternglanz, R. Role of NAD^+ in the deacetylase activity of the SIR2-like proteins. *Biochem. Biophys. Res. Commun.* **278,** 685–690 (2000).
18. Gasch, A. P. *et al.* Genomic expression programs in the response of yeast cells to environmental changes. *Mol. Biol. Cell* **11,** 4241–4257 (2000).
19. Sandmeier, J. J., Celic, I., Boeke, J. D. & Smith, J. S. Telomeric and rDNA silencing in *Saccharomyces cerevisiae* are dependent on a nuclear NAD^+ salvage pathway. *Genetics* **160,** 877–889 (2002).
20. Perichon, R., Bourre, J. M., Kelly, J. F. & Roth, G. S. The role of peroxisomes in aging. *Cell Mol. Life Sci.* **54,** 641–652 (1998).
21. Lin, S. J. *et al.* Calorie restriction extends *Saccharomyces cerevisiae* lifespan by increasing respiration. *Nature* **418,** 344–348 (2002).
22. Lin, S. S., Manchester, J. K. & Gordon, J. I. Enhanced gluconeogenesis and increased energy storage as hallmarks of aging in *Saccharomyces cerevisiae*. *J. Biol. Chem.* **276,** 36000–36007 (2001).
23. Unkefer, C. J. & London, R. E. *In vivo* studies of pyridine nucleotide metabolism in *Escherichia coli* and *Saccharomyces cerevisiae* by carbon-13 NMR spectroscopy. *J. Biol. Chem.* **259,** 2311–2320 (1984).
24. Grant, R. S. & Kapoor, V. Murine glial cells regenerate NAD, after peroxide-induced depletion, using either nicotinic acid, nicotinamide, or quinolinic acid as substrates. *J. Neurochem.* **70,** 1759–1763 (1998).
25. Aksoy, S., Szumlanski, C. L. & Weinshilboum, R. M. Human liver nicotinamide N-methyltransferase. cDNA cloning, expression, and biochemical characterization. *J. Biol. Chem.* **269,** 14835–14840 (1994).
26. Niewmierzycka, A. & Clarke, S. *S*-Adenosylmethionine-dependent methylation in *Saccharomyces cerevisiae*. Identification of a novel protein arginine methyltransferase. *J. Biol. Chem.* **274,** 814–824 (1999).
27. Virag, L. & Szabo, C. The therapeutic potential of poly(ADP-ribose) polymerase inhibitors. *Pharmacol. Rev.* **54,** 375–429 (2002).
28. Lal, A. *et al.* A public database for gene expression in human cancers. *Cancer Res.* **59,** 5403–5407 (1999).
29. Kassem, H., Sangar, V., Cowan, R., Clarke, N. & Margison, G. P. A potential role of heat shock proteins and nicotinamide N-methyl transferase in predicting response to radiation in bladder cancer. *Int. J. Cancer* **101,** 454–460 (2002).
30. Ghislain, M., Talla, E. & Francois, J. M. Identification and functional analysis of the *Saccharomyces cerevisiae* nicotinamidase gene, *PNC1*. *Yeast* **19,** 215–224 (2002).

Acknowledgements We thank members of the Sinclair laboratory, R. Veech, C. Wolberger, W. Forrester, S. Luikenhuis and D. Finkelstein, for reagents and discussions. This work was supported by the NIA and the Harvard–Armenise Foundation. D.S. is an Ellison Medical Research Foundation Special Fellow. R.A. is supported by a John Taplan Postdoctoral Fellowship, J.W. by a National Science Foundation Scholarship, and K.B. and O.M. by the American Federation of Aging Research.

Competing interests statement The authors declare that they have no competing financial interests.

Correspondence and requests for materials should be addressed to D.A.S. (david_sinclair@hms.harvard.edu).

Computational design of receptor and sensor proteins with novel functions

Loren L. Looger, Mary A. Dwyer, James J. Smith & Homme W. Hellinga

Department of Biochemistry, Duke University Medical Center, Durham, North Carolina 27710, USA

The formation of complexes between proteins and ligands is fundamental to biological processes at the molecular level. Manipulation of molecular recognition between ligands and proteins is therefore important for basic biological studies[1] and has many biotechnological applications, including the construction of enzymes[2–4], biosensors[5,6], genetic circuits[7], signal transduction pathways[8] and chiral separations[9]. The systematic manipulation of binding sites remains a major challenge. Computational design offers enormous generality for engineering protein structure and function[10]. Here we present a structure-based computational method that can drastically redesign protein ligand-binding specificities. This method was used to construct soluble receptors that bind trinitrotoluene, L-lactate or serotonin with high selectivity and affinity. These engineered receptors can function as biosensors for their new ligands; we also incorporated them into synthetic bacterial signal transduction pathways, regulating gene expression in response to extracellular trinitrotoluene or L-lactate. The use of various ligands

and proteins shows that a high degree of control over biomolecular recognition has been established computationally. The biological and biosensing activities of the designed receptors illustrate potential applications of computational design.

The general principles for the formation of specific complexes are well understood[11], and involve a lock-and-key fit between ligand and receptor, the structure of which is determined primarily by short-range interactions (steric contacts and hydrogen bonds). Complex formation is thermodynamically driven primarily by the hydrophobic effect and by long-range electrostatics. Difficulties in structure-based computational design arise from limitations in the description of the molecular interactions and the combinatorial complexity of the problem[12,13]. Despite notable advances in the rational manipulation of protein sequence and stability using automated computational design tools[12], the computational design of ligand-binding properties has been limited to metal centres[4], changes in specificity in which much of the chemical character of the wild-type ligand is retained[2,8,14] or has resulted in relatively weak binding[3].

Here we present a computational method for the redesign of ligand-binding-site specificity in proteins (see Supplementary Information for details). By using high-resolution three-dimensional structures, the algorithm identifies amino-acid sequences that are predicted to form a complementary surface between the protein and a target ligand replacing the wild-type ligand. The procedure combines target-ligand docking ($\sim 10^8$ translations and rotations) with mutations of amino-acid residues in direct contact with the wild-type ligand (typically 12–18 residues, corresponding to 10^{45} to 10^{68} mutant structures representing 10^{15} to 10^{23} sequences). The resulting combinatorial problem (10^{53} to 10^{76} choices) is solved with an algorithm based on the dead-end elimination (DEE) theorems[13]. This procedure deterministically identifies the global minimum of a semi-empirical potential function describing the molecular interactions in the system[13], including a modified Lennard-Jones potential, an explicit, geometry-dependent hydrogen-bonding term and a continuum solvation term to represent the hydrophobic effect. Additionally, a new term demanding that potential hydrogen-bond donors and acceptors in the ligand must be satisfied was found to be critical; it captures the necessity of balancing the hydrogen bond inventory, which is a dominant effect in molecular recognition[11]. Designs are selected for experimentation from a rank-ordered set of possibilities. The design process is relatively rapid, requiring about 3 days of computation to generate a set of designs in a particular protein for a given ligand on a 20-processor computer cluster.

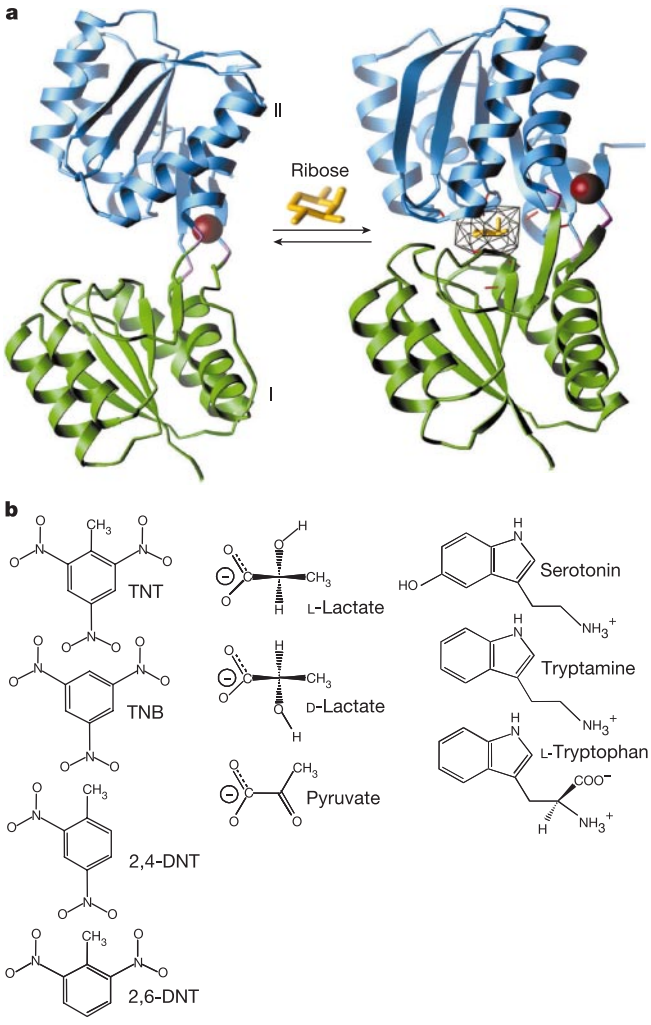

Figure 1 Structures of a representative receptor and all target ligands. **a**, Ribose binding mediates a transition from an open (left) to a closed (right) conformation[17]. The protein has two domains (I, amino terminal, green; II, carboxy terminal, blue), linked by a hinge region (H, purple). Fluorescence intensity changes of an environmentally sensitive, thiol-reactive fluorescent dye coupled to a mutant cysteine residue at position 265 (burgundy) monitor ligand binding[6]. Calculations use the closed structure, mutating the complementary surface residues (red) and docking the target ligands into the convex hull shown (black). **b**, Structures of target ligands and structurally related decoys used to probe the specificity of the designed receptors.

This procedure was used to engineer binding sites for trinitrotoluene (TNT), L-lactate or serotonin in place of the wild-type sugar or amino-acid ligands of five members of the *Escherichia coli* periplasmic binding protein (PBP) superfamily[15], using the high-resolution three-dimensional structures of the closed conformation of these proteins complexed with their wild-type ligand as starting points for the calculation (Fig. 1). The five proteins were glucose-binding protein (GBP)[16], ribose-binding protein (RBP)[17], arabinose-binding protein (ABP)[18], glutamine-binding protein (QBP)[19] and histidine-binding protein (HBP)[20]. The variation in structure and sequence[15] of these proteins presents distinct starting points for the design calculations. The three target ligands selected for this study bear little resemblance to the wild-type cognate ligands of the chosen PBPs; they are chemically distinct from each other and one of them (TNT) is a non-natural molecule. The designs therefore explore critical parameters of molecular recognition, including molecular shape, chirality, functional groups (hydrogen bonding, in terms of nitro (acceptor), hydroxyl (donor and acceptor) and carboxylate (acceptor); and molecular surface, in terms of polar, aliphatic and aromatic), internal flexibility (TNT < L-lactate < serotonin), charge (neutral (TNT), anionic (L-lactate) and cationic (serotonin)) and water solubility (TNT < serotonin < L-lactate).

Complementary surfaces were designed for TNT in RBP, ABP and HBP, for L-lactate in ABP, GBP, RBP, HBP and QBP, and for serotonin in ABP (Fig. 2, Table 1). The designed surfaces are electrically neutral for TNT, positively charged for lactate, and negatively charged for serotonin. Hydrophobic groups of all three target ligands interact primarily with aliphatic side chains, although several examples of aromatic interactions are seen (TNT.A1, TNT.H1, Lac.G1). In one instance, an example of dual aromatic stacking was obtained (TNT.R3). In all cases, the hydrogen-bonding potential (donor, acceptor) of the functional groups on the ligand is largely satisfied.

Seventeen designs predicted by the automated design procedure were selected for experimental characterization (Table 1). The predicted mutations (ranging from 5 to 17 amino-acid changes) were constructed by polymerase chain reaction mutagenesis of the wild-type receptor scaffold genes[6]. Proteins were overexpressed, purified and modified with thiol-reactive styryl dyes conjugated to cysteine residues introduced by mutation at locations where the fluorescence emission intensity of the dye responds to a ligand-mediated hinge-bending motion of the receptor[6]. Ligand-binding

affinities (Table 2) were determined by titration, monitoring ligand-dependent changes in fluorescence emission intensity that were fitted to single-site binding isotherms[6] (Supplementary Information). In all cases, wild-type receptors show no change in fluorescence intensity upon addition of target ligands. Conversely, the mutant receptors respond only to target and not wild-type ligands. A wide range of affinities is observed, down to the nanomolar level (TNT.R3). To probe the specificity of interaction, the affinities of several closely related ligands (Fig. 1b) were also determined (Table 2). The thermostabilities of a representative subset of apo-receptors (Supplementary Information) showed that cooperative folding transitions are retained with a slight loss of stability relative to the wild-type proteins.

Every designed receptor exhibits a detectable affinity for its target ligand. In the TNT designs, all six receptors can distinguish the absence of a single nitro group (2,4- and 2,6-dinitrotoluene) and, with the exception of the ABP design, the absence of a single methyl group (trinitrobenzene). The introduction of an additional point mutation suggested by visual inspection of the model to improve packing is sufficient to achieve the desired selectivity in this ABP design. All 10 lactate designs exhibit the desired chiral stereospecificity, selecting L-lactate over both the D-lactate enantiomer and pyruvate, the prochiral oxidized form of lactate. The single serotonin design has a significantly lower affinity for tryptamine (absence of a hydroxyl group) and tryptophan (absence of a hydroxyl group and presence of a carboxylate group). The relative free energy corresponding to the loss of a hydrogen bond in a decoy ligand (1–5 kcal mol^{-1}; Supplementary Information) is consistent with the observed range of weak and strong hydrogen bonds[11]. The automated computational design procedure therefore reliably predicts mutant receptors that attain ligand binding with the desired, drastically altered specificity, consistent with correct modelling of critical elements of molecular recognition: shape, functional groups and chirality.

The affinities of the wild-type receptors for their cognate ligands fall in the range 0.1–1.5 μM (ref. 6). Two of the three TNT designs in RBP also fall into this range (Table 2); the binding behaviour of these computationally designed receptors is therefore indistinguishable from naturally evolved PBPs. It has been observed that the maximal binding affinity for many ligands is correlated with the number of non-hydrogen atoms[21]. The affinity of one TNT design, TNT.R3, is 2 nM, corresponding to its empirically expected value. The single serotonin design does not attain the expected nanomolar affinity. The affinity of the fully automated design (Stn.A1) is 50 μM, and is improved to 4.7 μM by the introduction of a single point mutation predicted to improve packing interactions between receptor and ligand. Several of the lactate designs have micromolar affinities, approaching the expected maximum for a six-atom ligand (0.3 μM).

High-affinity receptors are successfully identified within the top 10 ranked designs for each ligand, corresponding to a tiny fraction of the available search space. Nevertheless, the designs exhibit a significant spread in ligand-binding affinities, not only for a given

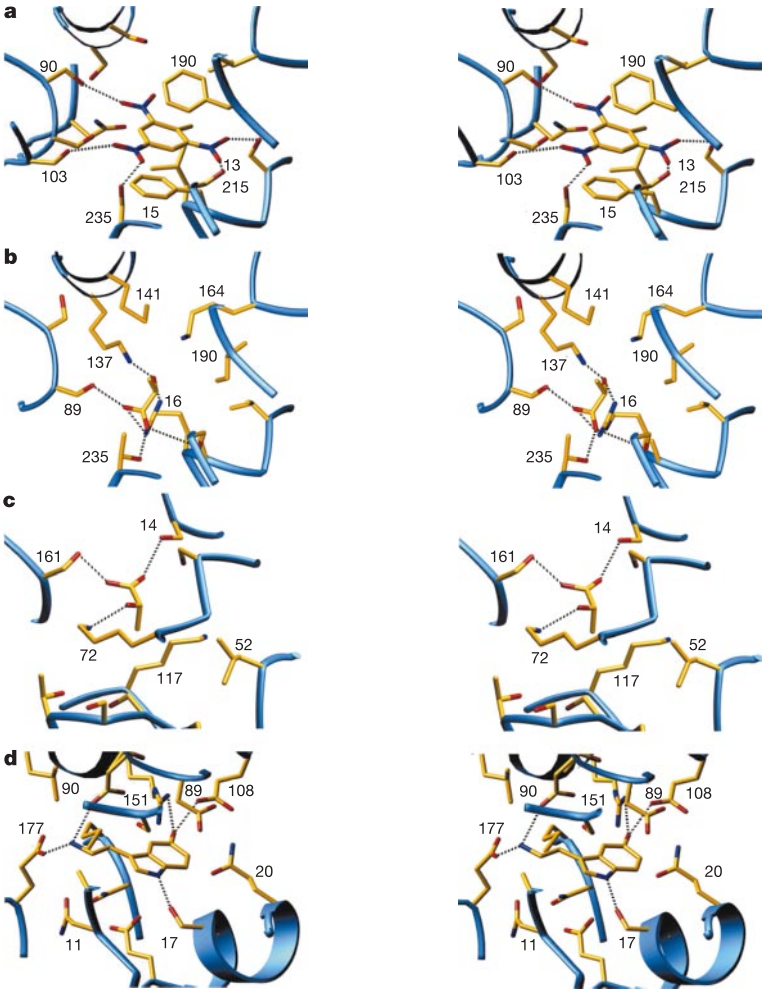

Figure 2 Stereo views of representative designed ligand-binding sites: **a**, TNT.R3; **b**, Lac.R1; **c**, Lac.H1; **d**, Stn.A1 (dashed lines indicate hydrogen bonds between protein and ligand; numbers identify side chains close to the ligand). TNT.R3 and Lac.R1 are presented in the same orientation, illustrating the adaptability of the RBP scaffold to bind different ligands. The Lac.R1 and Lac.H1 structures illustrate that the same ligand can be bound by sites designed in different scaffolds.

Table 1 **Complementary surface sequences of the designed receptors**

Scaffold	Target	Design	Complementary surface sequence†															
RBP			9_I	13_I	15_I	16_I	64_I	89_I	90_I	103_H	132_H	137_H	141_{II}	164_{II}	190_{II}	214_{II}	215_{II}	235_{II}
		Wild-type	S	N	F	F	N	D	R	S	I	A	R	F	N	F	D	Q
	TNT	R1 (I)	S	N	**A**	**N**	**S**	**S**	R				**T**	**S**	N		**A**	**S**
		R2 (I)	S	**I**	**A**	**N**	N	**A**	**D**		**K**		**A**	**N**	N	**K**	**A**	**N**
		R3 (A)		**S**	F	**L**		**S**	**S**	S		**S**	**S**	**I**	**F**		**S**	**S**
	Lac	R1 (A)		**V**	**A**	**R**		**S**	**S**	S		**K**	**M**	**K**	**I**		**S**	**T**
GBP			10_I	14_I	16_I	91_I	92_I	152_{II}	154_{II}	158_{II}	183_{II}	211_{II}	236_{II}	256_{II}				
		Wild-type	Y	D	F	N	K	H	D	R	W	N	D	N				
	Lac	G1(A)	**K**	**K**	F	**K**	**L**	**M**	**H**	**K**	**K**	N	A	**D**				
		G2(A)	**K**	**M**	**K**	**K**	**L**	**K**	**K**	**M**	**K**	N	A	**S**				
ABP			10_I	11_I	14_I	16_I	17_I	20_I	64_I	89_I	90_I	108_{II}	145_{II}	147_{II}	151_{II}	177_{II}	204_{II}	205_{II}	232_{II}	235_{II}
		Wild-type	K	Q	E	W	F	E	C	D	D	M	L	T	R	N	M	N	N	D
	TNT	A1(I)	**S**	**R**	**T**	**A**	**A**	**K**	**A**	**A**	**I**	R	**Q**	S	**D**	**L**	**A**		**F**	**T**
		A2‡ (I)	**S**	**R**	**T**	**A**	**A**	**K**	**S**	**A**	**I**	**R**	**Q**	S	**D**	**L**	**A**		**F**	**T**
	Lac	A1(A)	K		E	**Y**			**A**	**L**	**A**	**A**	**R**	S	S		**T**	N	**K**	
		A2(A)	K		**L**	**Y**			**A**	**S**	**S**	**A**	**R**	S	S		**T**	**K**	**H**	
	Stn	A1(I)	**A**	Q	E	**A**	**S**	**Q**	**S**	D	D	**E**	L	T	R	**E**	M	N	N	
		A2‡ (I)	**A**	Q	E	**A**	**S**	**Q**	**S**	D	**N**	**E**	L	T	R	**E**	M	N	N	
HBP			11_I	14_I	52_I	70_I	71_I	72_I	77_I	117_{II}	120_{II}	121_{II}	122_{II}	143_{II}	161_{II}					
		Wild-type	D	Y	L	S	L	S	R	L	T	T	Q	Q	D					
	TNT	H1(I)	**T**	**S**	**S**		**F**	**K**	R	**A**	**S**			Q	**S**					
		H2(I)	**N**	**A**	**N**		**Q**	**K**	R	L	T		Q	**T**	**N**					
	Lac	H1(A)		**S**	L	S		**K**	R	**K**	**S**	S	**T**		**S**					
		H2(A)		**S**	**K**	**T**		**K**	R	**H**	**S**	A	**T**		**T**					
QBP			10_I	13_I	50_I	70_I	75_I	115_{II}	118_{II}	156_{II}	157_{II}	185_{II}								
		Wild-type	D	F	F	T	R	K	T	H	D	Y								
	Lac	Q1(A)	D	**L**	**L**	**S**	R	K	T	H	**H**	**F**								
		Q2(A)	D	**R**	**S**	T	R	K	**S**	H	**R**	**F**								
		Q3(A)	D	**L**	**K**	**S**	**D**	K	T	H	**R**	**F**								

The Nomenclature for the designed receptors gives the target ligand and a single-letter abbreviation of the scaffold protein.
†Subscripts indicate the location of a residue position: I, N-terminal domain; II, C-terminal domain; H, hinge (Fig. 1). Bold letters indicate mutations from wild type (calculations may predict retention of wild-type residues). Underlined letters represent side chains making hydrogen bonds with the ligand (cognate ligand in the case of wild type). The design calculations in a given receptor were not always performed with identical complementary surface residues: automated identification of the complementary surface is indicated by 'A' (see Supplementary Information); 'I' indicates identification by inspection. Blanks therefore indicate residue positions not included in a calculation (wild-type sequence and conformation).
‡TNT.A2 is a point mutant of TN1.A1; Stn.A2 is a point mutant of Stn.A1. Both mutations were designed by inspection.

ligand in a particular scaffold, but also between scaffolds. The likelihood that a protein scaffold can be mutated to accept a new target ligand ('adaptive potential') is also variable. The observed range of affinities can be rationalized with an empirical quantitative structure–activity relationship (QSAR) that provides empirically fitted weights for the DEE force-field components (steric clashes and unsatisfied hydrogen bonds) and takes into account additional factors not modelled by the DEE force field (hydrophobic contact areas, electrostatics and volume ratio of wild-type to target ligands as a measure of adaptive potential; see Supplementary Information). This QSAR provides direct reciprocity between theory and experiment, completing the loop in the protein design cycle, and will be used in future experiments to select scaffolds on the basis of their predicted adaptive potential, and for rank-ordering designs by QSAR-based predicted affinities[22].

RBP and GBP control the chemotaxis of *E. coli* towards sugars, which is mediated by a two-component signal transduction pathway[23]. This response can be reconnected to gene regulation by constructing a synthetic signal transduction pathway that controls the transcriptional upregulation of a β-galactosidase reporter gene[24] (Fig. 3a). The biological activities of the TNT and L-lactate designs in RBP and the L-lactate designs in GBP were tested in this pathway, replacing wild-type RBP and GBP with designed receptors. Wild-type receptors mediate increases in reporter gene expression in response to ribose or glucose but not in response to TNT or L-lactate. Conversely, all the redesigned receptors respond to their target ligands but not to wild-type ligands. The dose–response

Table 2 **Affinities of the designed receptors for target ligands and analogues**

		K_d (μM)			
Target	Receptor	TNT	TNB	2,4-DNT	2,6-DNT
TNT	RBP.R1	0.34	1.0	5.0	5.4
	RBP.R2	1.6	3.8	5.3	4.9
	RBP.R3	0.002	0.1	8.4	15
	ABP.A1	1,400	600	>10,000	>10,000
	ABP.A2	400	500	2,000	4,000
	HBP.H1	220	1,000	>10,000	>10,000
		L-Lac		D-Lac	Pyr
L-Lactate	GBP.G1	2.8		205	255
	GBP.G2	2.1		55	115
	HBP.H1	1.8		40	50
	HBP.H2	12.2		30	48
	QBP.Q1	9,500		>100,000	>100,000
	QBP.Q2	300		>100,000	>100,000
	QBP.Q3	25,000		>100,000	>100,000
	ABP.A1	160		>100,000	>100,000
	ABP.A2	20,000		>100,000	>100,000
	RBP.R1	7.4		40	40
		Stn		Trp	Trm
Serotonin	ABP.A1	50		660	900
	ABP.A2	4.7		65	90

The limit of detection for the nitro compounds corresponds to affinities of ~10 mM, and for lactate analogues to 100 mM. Error of K_d measurement is approximately 10% (see Supplementary Information). TNB, trinitrobenzene; DNT, dinitrobenzene; Pyr, pyruvate, Stn, serotonin; Trp, L-tryptophan; Trm, tryptamine.

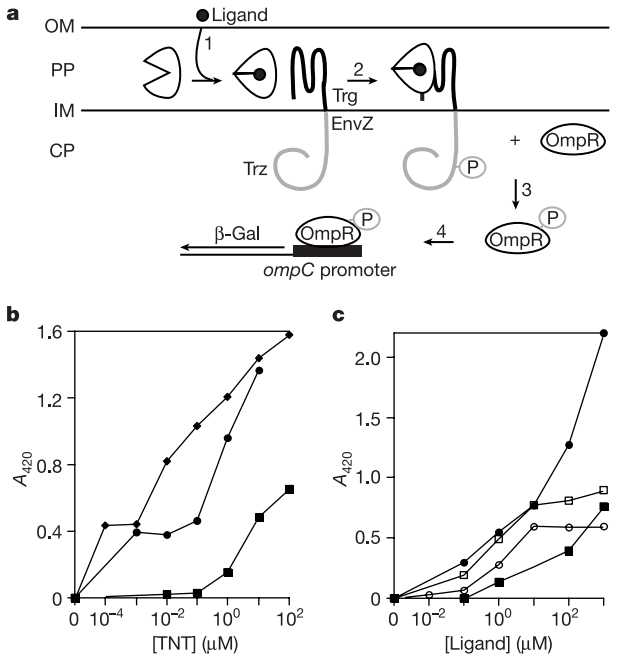

Figure 3 Synthetic two-component signal transduction pathway[24]. **a**, The ligand-bound RBP or GBP (1) interacts with the Trg domain (thick black line) of a chimaeric transmembrane histidine kinase, Trz (2), resulting in autophosphorylation of the EnvZ domain (grey line) and phosphate transfer to OmpR (3), which then binds to the *ompC* promoter (4), upregulating *lacZ* transcription. OM, outer membrane; PP, periplasm; IM, inner membrane; CP, cytoplasm. **b**, Response to TNT (circles, TNT.R1; squares, TNT.R2; diamonds, TNT.R3). **c**, Response to sugar (open circles, ribose and wild-type RBP; open squares, glucose and wild-type GBP) and L-lactate (filled circles, Lac.R1; filled squares, Lac.G1). β-Galactosidase activities are reported as the difference in assay end-point absorbances of ligand-stimulated and unstimulated cultures. Sensitivity of *E. coli* to high TNT or L-lactate concentrations precluded the determination of full dose–response curves. There was no response in the absence of receptors or *trz*.

curves of the TNT-binding RBP receptors follow the same order as the intrinsic ligand-binding affinities (Fig. 3b, c). The redesigned receptors therefore mediate signal transduction to extracellular TNT or L-lactate, as intended.

We have shown that binding specificities of receptors can be changed drastically by a computational design algorithm. The receptors bind their new cognate ligands selectively relative to closely related decoy molecules, and have affinities that in several cases rival or exceed the affinities of the naturally evolved parent proteins. Essential elements of molecular recognition are therefore correctly captured by the computational design process. The method is relatively rapid and can be applied to many different ligands and proteins. Several of the designed receptors are biologically active, showing that computational design can be used successfully to manipulate biological systems. Furthermore, even within the relatively small number of examples presented here, several potential biotechnological applications are illustrated. The engineered PBPs have the appropriate affinities and specificities for use as reagentless fluorescent biosensors[5,6] or cell-based sensors[25], although further work will be needed to develop devices capable of being deployed in the field. TNT is a potent carcinogen as well as an explosive, and contaminates soil and water near military installations[26]. The TNT.R3 receptor represents a first step in the development of reagentless fluorescent sensors to detect the source of underwater TNT plumes that leach into the sea from unexploded ordnance in coastal waters, using plume-tracing underwater robotic vehicles[27]. On land there is an urgent need to detect landmines[26]. Vapour-phase TNT chemical sensors have been developed successfully[28]. However, spraying mined fields with bacteria that respond to TNT by transcriptional activation of a fluorescent reporter gene might offer advantages in cost and simplicity[29]. The bacterial signal transduction system driven by the engineered TNT.R3 receptor illustrates the potential for developing specific cell-based detectors for chemical threats and pollutants. The L-lactate and serotonin receptors also have practical applications in clinical chemistry. Elevated concentrations of L-lactate are indicative of several medical conditions[30]. Fluctuations in serotonin blood concentrations are associated with a variety of psychiatric conditions, and elevated concentrations indicate the presence of certain bowel tumours[30]. The computational design of chirally selective receptors, illustrated by the L-lactate case, could be of use in the facile chromatographic preparation of optically pure pharmaceuticals from racemic mixtures, which is important for drug development[9]. In principle, the computational design strategy presented here can be extended to the design of enzymes[3,4]. □

Received 4 September 2002; accepted 10 March 2003; doi:10.1038/nature01556.

1. Bishop, A. *et al.* Unnatural ligands for engineered proteins: new tools for chemical genetics. *Annu. Rev. Biophys. Biomol. Struct.* **29,** 577–606 (2000).
2. Harris, J. L. & Craik, C. S. Engineering enzyme specificity. *Curr. Opin. Chem. Biol.* **2,** 127–132 (1998).
3. Bolon, D. N. & Mayo, S. L. Enzyme-like proteins by computational design. *Proc. Natl Acad. Sci. USA* **98,** 14274–14279 (2001).
4. Benson, D. E., Haddy, A. E. & Hellinga, H. W. Converting a maltose receptor into a nascent binuclear oxygenase by computational design. *Biochemistry* **41,** 3262–3267 (2002).
5. Hellinga, H. W. & Marvin, J. S. Protein engineering and the development of generic biosensors. *Trends Biotechnol.* **16,** 183–189 (1998).
6. de Lorimier, R. M. *et al.* Design, construction and analysis of a family of fluorescent biosensors. *Protein Sci.* **11,** 2655–2675 (2002).
7. Hasty, J., McMillen, D. & Collins, J. J. Engineered gene circuits. *Nature* **420,** 224–230 (2002).
8. Koh, J. T. Engineering selectivity and discrimination into ligand–receptor interfaces. *Chem. Biol.* **9,** 17–23 (2002).
9. Maier, N. M., Franco, P. & Lindner, W. Separation of enantiomers: needs, challenges, perspectives. *J. Chromatogr. A* **906,** 3–33 (2001).
10. Arnold, F. H. Combinatorial and computational challenges for biocatalyst design. *Nature* **409,** 253–257 (2001).
11. Fersht, A. R. *Structure and Mechanism in Protein Science* (Freeman, New York, 1999).
12. Dahiyat, B. I. & Mayo, S. L. *De novo* protein design: Fully automated sequence selection. *Science* **278,** 82–87 (1997).
13. Looger, L. L. & Hellinga, H. W. Generalized dead-end elimination algorithms make large-scale protein side-chain structure prediction tractable: implications for protein design and structural genomics. *J. Mol. Biol.* **307,** 429–445 (2001).
14. Reina, J. *et al.* Computer-aided design of a PDZ domain to recognize new target sequences. *Nature Struct. Biol.* **9,** 621–627 (2002).
15. Tam, R. & Saier, M. H. Jr. Structural, functional, and evolutionary relationships among extracellular solute-binding receptors of bacteria. *Microbiol. Rev.* **57,** 320–346 (1993).
16. Vyas, M. N., Vyas, N. K. & Quiocho, F. A. Crystallographic analysis of the epimeric and anomeric specificity of the periplasmic transport/chemosensory protein receptor for D-glucose and D-galactose. *Biochemistry* **33,** 4762–4768 (1994).
17. Mowbray, S. L. & Cole, L. B. 1.7 Å X-ray structure of the periplasmic ribose receptor from *Escherichia coli*. *J. Mol. Biol.* **225,** 155–175 (1992).
18. Quiocho, F. A. & Vyas, N. K. Novel stereospecificity of the L-arabinose-binding protein. *Nature* **310,** 381–386 (1984).
19. Sun, Y. J., Rose, J., Wang, B. C. & Hsiao, C. D. The structure of glutamine-binding protein complexed with glutamine at 1.94 Å resolution: comparisons with other amino acid binding proteins. *J. Mol. Biol.* **278,** 219–229 (1998).
20. Yao, N., Trakhanov, S. & Quiocho, F. A. Refined 1.89 Å structure of the histidine-binding protein complexed with histidine and its relationship with many other active transport/chemosensory proteins. *Biochemistry* **33,** 4769–4779 (1994).
21. Kuntz, I. D., Chen, K., Sharp, K. A. & Kollman, P. A. The maximal affinity of ligands. *Proc. Natl Acad. Sci. USA* **96,** 9997–10002 (1999).
22. Dahiyat, B. I. & Mayo, S. L. Protein design automation. *Protein Sci.* **5,** 895–903 (1996).
23. Stock, A. M., Robinson, V. L. & Goudreau, P. N. Two-component signal transduction. *Annu. Rev. Biochem.* **69,** 183–215 (2000).
24. Baumgartner, J. W. *et al.* Transmembrane signalling by a hybrid receptor: communication from the domain of chemoreceptor Trg that recognizes sugar-binding proteins to the kinase/phosphatase domain of osmosensor. *EnvZ. J. Bacteriol.* **176,** 1157–1163 (1994).
25. Daunert, S. *et al.* Genetically engineered whole-cell sensing systems: coupling biological recognition with reporter genes. *Chem. Rev.* **100,** 2705–2738 (2000).
26. Yinon, Y. Field detection and monitoring of explosives. *Trends Anal. Chem.* **21,** 292–301 (2002).
27. Mead, K. S. Using lobster noses to inspire robot sensor design. *Trends Biotechnol.* **20,** 276–277 (2002).
28. Cumming, C. L. *et al.* Using novel fluorescent polymers as sensory materials for above-ground sensing of chemical signature compounds emanating from buried land mines. *IEEE Trans. Geosci. Remote Sens.* **39,** 1119–1128 (2001).
29. Burlage, R. S., Patek, D. R. & Everman, K. R. Method for detection of buried explosives using a biosensor. US patent 5,972,638 (1999).
30. Burtis, C. A. & Ashwood, E. R. *Tietz Textbook of Clinical Chemistry* (Saunders, London, 1999).

Supplementary Information accompanies the paper on **www.nature.com/nature**.

Acknowledgements We thank M. Inouye for the gift of the RU1012 strain, L. Loew for the gift of styryl dyes, S. Conrad and G. Shirman for assistance with mutagenesis and protein chemistry, and M. G. Prisant for construction of the computer cluster. This work was supported by grants from the Office of Naval Research, the Defense Advanced Research Project Agency and the National Institutes of Health.

Competing interests statement The authors declare that they have no competing financial interests.

Correspondence and requests for material should be addressed to H.W.H. (hwh@biochem.duke.edu).

Direct observation of catch bonds involving cell-adhesion molecules

Bryan T. Marshall*, Mian Long*†, James W. Piper*†, Tadayuki Yago‡, Rodger P. McEver‡§ & Cheng Zhu*‖

** Woodruff School of Mechanical Engineering and ‖ Coulter School of Biomedical Engineering, Georgia Institute of Technology, Atlanta, Georgia 30332, USA*
‡ Cardiovascular Biology Research Program, Oklahoma Medical Research Foundation, and § Department of Biochemistry and Molecular Biology and Oklahoma Center for Medical Glycobiology, University of Oklahoma Health Sciences Center, Oklahoma City, Oklahoma 73104, USA

Bonds between adhesion molecules are often mechanically stressed. A striking example is the tensile force applied to selectin–ligand bonds, which mediate the tethering and rolling of flowing leukocytes on vascular surfaces[1–3]. It has been suggested that force could either shorten bond lifetimes, because work done by the force could lower the energy barrier between the bound and free states[4] ('slip'), or prolong bond lifetimes by deforming the molecules such that they lock more tightly[5,6] ('catch'). Whereas slip bonds have been widely observed[7–14], catch bonds have not been demonstrated experimentally. Here, using atomic force microscopy and flow-chamber experiments, we show that increasing force first prolonged and then shortened the lifetimes of P-selectin complexes with P-selectin glycoprotein ligand-1, revealing both catch and slip bond behaviour. Transitions between catch and slip bonds might explain why leukocyte rolling on selectins first increases and then decreases as wall shear stress increases[9,15,16]. This dual response to force provides a mechanism for regulating cell adhesion under conditions of variable mechanical stress.

Using atomic force microscopy (AFM) (Fig. 1a), we measured the force dependence of bond lifetimes of P-selectin with two forms of P-selectin glycoprotein ligand-1 (PSGL-1) or with G1, a blocking monoclonal antibody (mAb) against P-selectin[17] (see Methods). P-selectin is an extended C-type lectin expressed on activated endothelial cells and platelets. PSGL-1 is a mucin expressed on leukocytes. Ca^{2+}-dependent interactions of P-selectin with PSGL-1 mediate the tethering and rolling of flowing leukocytes on vascular surfaces in response to infection or tissue injury[1–3].

We captured dimeric PSGL-1 purified from human neutrophils[18] or monomeric recombinant soluble PSGL-1 (sPSGL-1)[19] with PL2, a non-blocking anti-PSGL-1 mAb[20] adsorbed on the cantilever tip (Fig. 1b). Cantilever tips bearing (s)PSGL-1 or G1 were repeatedly brought into contact with lipid bilayers reconstituted with P-selectin purified from human platelets[21] to allow bond formation. The cantilever was then retracted a prescribed distance to apply a constant tensile force to the bond or bonds (if any resulted from the contact), and the duration or lifetime of the adhesion at that force was recorded (Fig. 1c). To measure lifetime at forces lower than the level of their fluctuations, many instantaneous forces were averaged (Fig. 1d, e). This enabled the reliable resolution of mean forces as low as a few piconewtons, and allowed the detected differences in mean forces to achieve high statistical significance (Fig. 1f). The binding frequency was kept low (12–20%) to ensure that most (about 90%) adhesions dissociated as a single step (Fig. 1c, lower tracing). Only single-step dissociations were analysed.

Binding was highly specific. Rendering the cantilever tip functional with (s)PSGL-1 increased adhesion frequencies 3–10-fold (Fig. 2a and b) and also increased bond lifetimes (Fig. 3a and b). The inclusion of blocking mAbs against P-selectin (G1) or against PSGL-1 (PL1[20]) or the divalent-cation chelator EDTA in the chamber solution decreased adhesion to nonspecific levels. G1-coated cantilever tips had significantly higher adhesion frequencies and longer bond lifetimes than control PL2-coated tips (Figs 2c and 3c).

Remarkably, both the P-selectin–sPSGL-1 interaction (Fig. 3a) and the P-selectin–PSGL-1 interaction (Fig. 3b) exhibited a biphasic relationship between lifetime and force. The bond lifetimes initially increased with force, indicating the presence of catch bonds. After reaching a maximum, the lifetimes decreased with force, indicating slip bonds. This biphasic pattern was detected in individual experiments with a single cantilever tip on a single bilayer, which included as few as about five lifetime measurements to calculate a mean and a standard deviation at each of four force levels to cover the biphasic region. This pattern remained unchanged as more data were accumulated (about 400 lifetime measurements for each form of PSGL-1), which allowed us to examine the distributions of lifetimes. As with published flow-chamber data[7,9,11–13], lifetimes at a given force seemed to follow an exponential distribution, which was made linear by plotting ln(number of events with a lifetime of t or more)

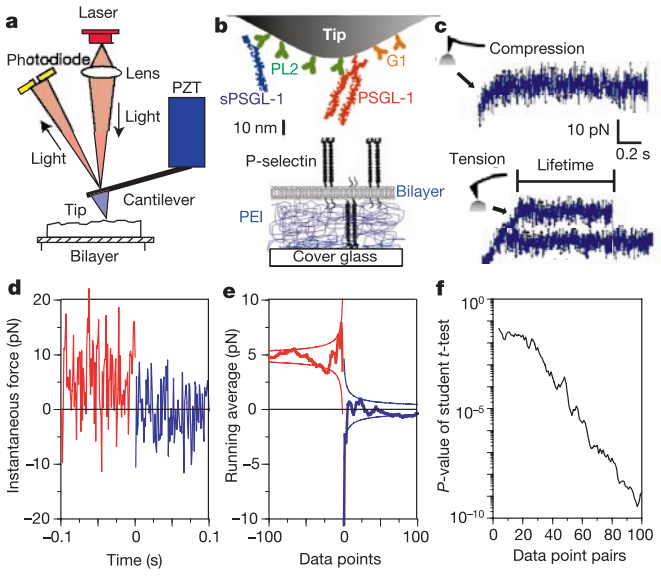

Figure 1 AFM system. **a**, Schematic diagram. **b**, Making the AFM functional. The cantilever tip depicted represents a composite of all molecules adsorbed or captured. sPSGL-1 and PSGL-1 are depicted as monomer and dimer, respectively. **c**, Force-scan curves illustrating the cantilever bending (insets) when a compressive or tensile force was applied to the tip. The upper curves illustrate a contact cycle without binding, where the retraction curve (from left to right) retraced the approach curve (from right to left). The lower curves illustrate a contact cycle with binding and lifetime measurement. **d**, Plot of instantaneous force against time before (red) and after (blue) an unbinding event. **e**, Running means (thick curves) ± s.e.m. (paired thin curves) against number of data points. **f**, P value of the Student's t-test comparing the difference of the two running means against numbers of point pairs.

† Present addresses: National Microgravity Laboratory, Institute of Mechanics, Chinese Academy of Sciences, Beijing 100080, China (M.L.), and Immucor, Inc., Norcross, Georgia 30091, USA (J.W.P.).